Hindawi
International Journal of Electrochemistry
Volume 2023, Article ID 7977453, 17 pages
https://doi.org/10.1155/2023/7977453

Research Article

Size-Dependent Chlorinated Nitrogen-Doped Carbon Nanotubes: Their Use as Electrochemical Detectors for Catechol and Resorcinol

Winny Kgabo Maboya[1] **and Mologadi Nkiyasi Rantho**[2]

[1]*Department of Biotechnology and Chemistry, Faculty of Applied and Computer Sciences, Vaal University of Technology, Private Bag X021, Vanderbijlpark 1900, South Africa*
[2]*Department of Physics, Mathematics and Non-Destructive Testing, Faculty of Applied and Computer Sciences, Vaal University of Technology, Private Bag X021, Vanderbijlpark 1900, South Africa*

Correspondence should be addressed to Winny Kgabo Maboya; winnyma@vut.ac.za

Received 3 May 2023; Revised 1 July 2023; Accepted 14 July 2023; Published 24 July 2023

Academic Editor: Hamish Andrew Miller

In this study, various-sized nitrogen-doped carbon nanotubes (NCNTs) were fabricated by varying the concentration of chlorine in the feed. The diameter of the NCNTs was found to influence the sensing ability of the nanomaterials when coated onto the glassy carbon electrode (GCE) and used for the detection of catechol (CC) and resorcinol (RS). Larger diameter NCNTs (denoted NCNTs (2 : 1)) were produced when a low concentration of chlorine was added into the acetonitrile feed, whereas smaller diameter NCNTs (denoted NCNTs (1 : 2)) were produced when a large concentration of chlorine was added. This investigation revealed that the addition of controllable amounts of chlorine during the fabrication of NCNTs led to the creation of nanostructures with different properties. The greatest current response which was evidenced by an enhanced anodic peak of CC and RS was obtained when GCE was coated with NCNTs (2 : 1), and this was attributed to their large diameter and high graphitic nature which facilitated electron transfer as evidenced by scanning electron microscopy (SEM), Raman spectroscopy, and X-ray photoelectron spectroscopy (XPS) analysis. A linear response was obtained when varying the concentration of both CC and RS, with the limits of detection of about 0.059 μM (CC) and 0.034 μM (RS) (3S/M) obtained.

1. Introduction

Phenol and its derivatives are widely used in many fields, such as tanning, cosmetic, dye, chemical, and pharmaceutical industries [1, 2]. These compounds contain aromatic rings with one or more hydroxyl groups functionalized on the carbon atom, ranging from simple phenols to high molecular weight polymers. Therefore, the development of methods that can be used for sensitive and selective monitoring of phenolic compounds is very important for environmental protection [3, 4]. Catechol (CC) and resorcinol (RS), together with hydroquinone (HQ), are a class of phenolic compounds called dihydroxybenzene isomers and are extensively used as chemical intermediates in the manufacture of many products, such as pesticides, agrochemicals, dyes, cosmetics, food additives, medicines, insecticides, and explosives [5–7]. These phenolic compounds are known as one of the significant threats for environmental pollutants because of their poor degradability and strong toxicity in nature [8, 9]. Traces of CC and RS are widely distributed in our ecosystem, for example, in our water sources, and they usually coexist as pollutants [10–12]. It is known that CC can produce renal tube destruction, liver function reduction, and strong central nervous system suppression when adsorbed in the gastrointestinal tract at high doses [13]. On the other hand, prolonged exposure to RS resulted in suppression of thyroid hormone synthesis in humans, haematological abnormalities, carcinogenesis, and fatal cases of human fetus poisoning [14]. As such, catechol is considered more toxic than resorcinol, and both are

considered more toxic than phenol [15, 16]. Catechol is fatally toxic to fish at concentrations of 5–25 mg/L [17], and it has been detected in wastewater from coal conversion processes (its concentration may be as high as 5300 mg/L at low temperature wastewater) [18], crude wood tar and drainage water from bituminous shale, and water from coal carbonization and gasification [19].

Phenols and associated compounds have been listed as priority pollutants by the Ministry of Environment and Forests (MoEF), the Government of India, and the United States Environmental Protection Agency (USEPA). As a result, Environmental Protection Agency (EPA) regulations call for controlling the level of these phenolic compounds to <1 ppm in wastewater [20]. In a quest to alleviate these hazardous compounds in water, effective and real-time monitoring of phenolic compounds using methods such as capillary electrophoresis [21], spectrophotometry [22], chromatography analysis [23], and electrochemical analysis has been explored.

Electrochemical techniques have recently drawn more attention as the detectors of choice due to their characteristic of being low cost, fast, simple, less time-consuming, and sensitive [24, 25]. However, since CC and RS are isomers, which may result in the overlap of their oxidation peaks, there are still challenges in simultaneously distinguishing and detecting CC and RS using bare electrodes. To solve this problem, researchers have developed new efficient and sensitive materials for simultaneously detecting dihydroxybenzenes by coating the surface of working electrodes with various carbon-based nanomaterials with excellent electronic transfer rate and good stability [26]. Among the developed carbon-based nanomaterials, multiwalled carbon nanotubes (MWCNTs) have aroused widespread attention [27]. Reports have surfaced on the use of surface-modified and heteroatom-doped MWCNTs coated on working electrode materials as electrochemical sensors for catechol with fewer studies on the detection of catechol in the presence of resorcinol [11, 28–37].

The oxygen-plasma-treated CNTs which were modified onto a GCE surface showed excellent electrochemical behaviour for the detection of catechol with the detection limit of 0.60 μM and exhibited long-term stability [28]. An electrochemical sensor based on fluorine and nitrogen codoped carbon dots decorated laccase was fabricated and used for the detection of catechol, with a low detection limit of 0.014 μM and sensitivity of 219.17 $\mu A \cdot cm^{-2} \cdot mM^{-1}$ obtained [29]. Oxygen-plasma-treated CNT electrodes were used for the detection of catechol, and it was found that this electrode had better electrochemical performance for the analysis of catechol than that of as-synthesized CNT electrode and exhibited long-term stability [30]. Samarium oxide decorated functionalized multiwall CNTs were used as electrode material for the detection of catechol with a low detection limit of 0.03 μM obtained and recovery of 94.5 to 99% in water samples [31]. A carbon paste electrode modified with the poly(sulfosalicylic acid) and multiwalled carbon nanotubes (MWCNTs) composite was constructed and used as an electrochemical sensor for catechol, and low detection limits of 0.16 μM were obtained [32]. An electrochemical sensor based on modification of GCE by the composite containing temperature-responsive polymer polystyrene-poly-N, N-diethyl acrylamide-polystyrene (PS-PDEA-PS), and fullerenes carboxylate multiwalled carbon nanotubes (C_{60}-MWCNTs) was fabricated and used for the detection of catechol [33]. The detection limit obtained for catechol was 1.45 μM, and the sensor possessed good stability and reproducibility [33]. A sensitive electrochemical sensor for catechol based on multiwalled carbon nanotubes poly(1,5-diaminonaphthalene) composite modified GCE which showed a low detection limit of 0.01 μM for catechol has been reported [34]. A novel catechol sensor fabricated from double layers of functionalized multiwalled carbon nanotubes coated with zinc oxide on a glassy carbon electrode showed a low detection limit of 0.027 μM for catechol [35]. An electrochemical sensor for catechol and nitrite based on gold nanoparticles (AuNPs) deposited on chitosan@N,S codoped multiwalled carbon nanotubes composite modified GCE was fabricated and exhibited low detection limits of 0.2 μM for both catechol and nitrite [36]. A surfactant-modified graphene paste electrode designed for the determination of catechol in the presence of resorcinol was developed, and the detection limit for catechol was found to be 0.106 μM [37]. A flexible composite paper Fe-Cu-based metal-organic framework/reduced graphene oxide electrode was prepared for the simultaneous detection of catechol and resorcinol, with detection limits of 0.016 and 0.020 μM, respectively [11].

In our previous studies, we have evaluated the role of chlorine addition during carbon nanomaterials (CNMs) synthesis in the presence and absence of nitrogen sources using catalytic vapour deposition (CVD) injection and bubbling methods on the morphology of the CNMs [38, 39]. From the reported literature, we expected the addition of chlorine to (i) result in an increase in the growth rate of the CNTs, (ii) aid in the purification of the carbon nanomaterials, and (iii) increase the amount of nitrogen doped into the carbon nanostructures. In our previous study, we also found that chlorine increased the growth rate of the CNTs, and that varying the amount of chlorine in the feed containing a nitrogen source using an injection CVD method, resulted in the formation of open-ended and closed-ended CNTs of variable morphologies [39]. Materials synthesized with the addition of large concentrations of chlorine in the feed also appeared more cleaner and were highly graphitic [39] while the synthesis of CNTs by adding only chlorine vapour to the CVD reactor containing the catalyst resulted in the creation of CNTs that had defects on the outer walls which in turn facilitated the growth of secondary carbon nanofibers at their walls [38]. In the present study, we needed to clarify the role of chlorine concentration further on the growth rate, morphology, purifying ability, and electrochemical response of nitrogen-doped carbon nanotubes using a bubbling CVD method.

To the best of our knowledge, there are no reports on the electrochemical detection of dihydroxybenzene isomers using a GCE modified with chlorinated N-doped CNTs, specifically the role of the size of the carbon nanomaterials on the sensing capability.

2. Experimental Section

2.1. Reagents. Acetonitrile (CH_3CN, ≥99.8%, Labchem), iron (III) nitrate nonahydrate ($Fe(NO_3)_3{\cdot}9H_2O \geq 98\%$, Kayla Africa Suppliers and Distributors), cobalt (II) nitrate hexahydrate ($Co(NO_3)_2{\cdot}6H_2O \geq 98\%$, Kayla Africa Suppliers and Distributors), calcium carbonate ($CaCO_3 \geq 99\%$, Glassworld), nitric acid ($HNO_3 \geq 98\%$ ACS, Kayla Africa Suppliers and Distributors), 1,2-dichlorobenzene ((Inqaba Biotechnical Industries, DCB) ≥ 99% Reagent plus), phosphate buffer saline tablets (Separations, pH 7.2), resorcinol (Inqaba Biotechnical Industries), catechol (Labchem), hydroquinone (Inqaba Biotechnical Industries), Al_2O_3 (0.3 μm, Bruno Steiner Lab Consultancy), dimethyl formamide (DMF, Kayla Africa Suppliers and Distributors), and polyvinylidene fluoride (PVDF, Sigma Aldrich) were used. All reagents were commercially available and used without further purification.

2.2. Fabrication of Chlorinated N-Doped CNTs by Bubbling CVD Method. About 1.0 g of a 10% Fe-Co/$CaCO_3$ catalyst, which was prepared using a method by Mhlanga et al. [40], was weighed and added to the quartz boat (purchased from Protea Laboratory Solutions), which was then placed in the centre of a quartz tube. Nitrogen (N_2, purchased from Afrox) was used as a carrier gas at a flow rate of 240 mL/min, while acetylene (C_2H_2, purchased from Afrox) was used as a source of carbon at a flow rate of 90 mL/min. The flow rates used were adopted from a method by Tetana et al. [41]. In the beginning, the furnace (which was custom-made at the University of the Witwatersrand) was gradually heated to 800°C at a heating rate of 10°C/min under flowing N_2 (50 mL/min). After the temperature of the furnace reached 800°C, the N_2 flow was adjusted to 240 mL/min, and the C_2H_2 gas was also opened (flowing at a flow rate of 90 mL/min), and both gases were bubbled into a mixture of acetonitrile and dichlorobenzene of various volume ratios, and the vapours created were flown into the CVD reactor. After 60 min of reaction, the system was left to cool to room temperature under a continuous flow of N_2 (50 mL/min). The quartz boat was then removed from the reactor, and the carbon deposit that formed was weighed. The carbon deposit was purified in 30% nitric acid (HNO_3), by stirring under reflux at 100°C for 1 hour, and this was followed by filtration of the material until the pH of the filtrates reached about 7. The resultant purified material was then dried in an oven overnight at 100°C.

2.3. Modification of GCE with Chlorinated N-Doped CNTs and Electrochemical Tests. The glassy carbon electrode (GCE) was cleaned before modification with chlorinated N-doped CNTs. The GCE was first polished with Al_2O_3 (0.3 μm) powder on a polishing cloth. This was followed by rinsing the GC electrode with deionized water, which was followed by sonication for 10 minutes in the following solvents: HNO_3 (1 : 1) acid solution, ethanol, and finally distilled water. The above cleaning procedure was repeated several times until a shiny surface was obtained on the GC electrode. Chlorinated N-doped CNTs suspension was prepared by mixing and dispersing 6 mg of chlorinated N-doped CNTs and 1 mg of PVDF in 400 μL dimethyl formamide (DMF) with the acid of ultrasonic agitation. About 50 μL of the chlorinated N-doped CNTs suspension was dropped onto the surface of a polished GCE, and the solvent was evaporated in an oven at 40°C. The procedure was repeated two times, meaning the electrode was coated two times. Cyclic voltammetry (CV) and differential pulse voltammetric (DPV) experiments were carried out in an electrochemical cell containing 10 mL of a 0.1 M phosphate buffer solution (PBS, pH 7.2) prepared at room temperature as the supporting electrolyte, and the scan rate used for CV was $50\ mV{\cdot}s^{-1}$. A 0.020 mol/L stock solution of analytes (CC, HQ, and RS) was prepared in distilled water using 10 mL volumetric flasks. For DPV, the parameters were as follows: amplitude, P_H (50 mV); pulse width, P_W (60 mV); potential step, S_H (10 mV); limit potential, E_V (0.6 V); and step time, S_T (200 ms). The detailed electrode preparation procedure and electrochemical testing are presented in Scheme 1.

2.4. Characterization. Transmission electron microscopy (TEM) (T12 FEI TECNAI G^2 SPIRIT) operating at 120 kV and scanning electron microscopy (SEM) (FEI Quanta 200) were utilized for the determination of the acid-purified and unpurified nanostructures morphology and their size distribution. For TEM, the nanostructure materials were sonicated in ethanol and deposited onto a holey carbon-coated TEM Cu grid once the homogeneous mixture was obtained. For SEM, the nanostructured materials were poured onto a tape that was attached to an SEM stub. The nanostructured materials on the stub were first coated with carbon, followed by gold-palladium to prevent them from charging. Raman spectroscopy (Jobin-Yvon T6400 micro-Raman spectrometer) was used to deduce the crystallinity of the nanostructured materials, where excitation was provided by the 514 nm green laser and a spectral resolution of $3–5\ cm^{-1}$. The amount of residues and other impurities present before and after acid purification of the nanostructured materials was determined by thermogravimetric analysis (TGA) (Perkin Elmer TGA 7). This was achieved by loading the nanostructured material sample onto a platinum pan, and the sample was heated to 900°C at a heating rate of 5°C/min, in a flowing air stream at 20 mL/min. The binding energy and nitrogen environments and their quantities in the nanostructured materials were evaluated using X-ray photoelectron spectroscopy (XPS) (Kratos Analytical (UK) provided by Rhodes University) with an AXIS Ultra DLD with an Al (monochromatic) anode equipped with a charge neutralizer. Electrochemical detection of analytes and the response behaviour of GC-coated electrodes were performed using cyclic voltammetry and differential pulse voltammetry (Biologic SP-240, Potentiostat (Bruno Steiner Laboratory Consultancy), operated by EcLab software). A glassy carbon working electrode ($A = 0.07\ cm^2$), platinum wire which acted as a counter electrode, and Ag/AgCl (3 M NaCl) which was used as a reference electrode were used in the electrochemical analysis.

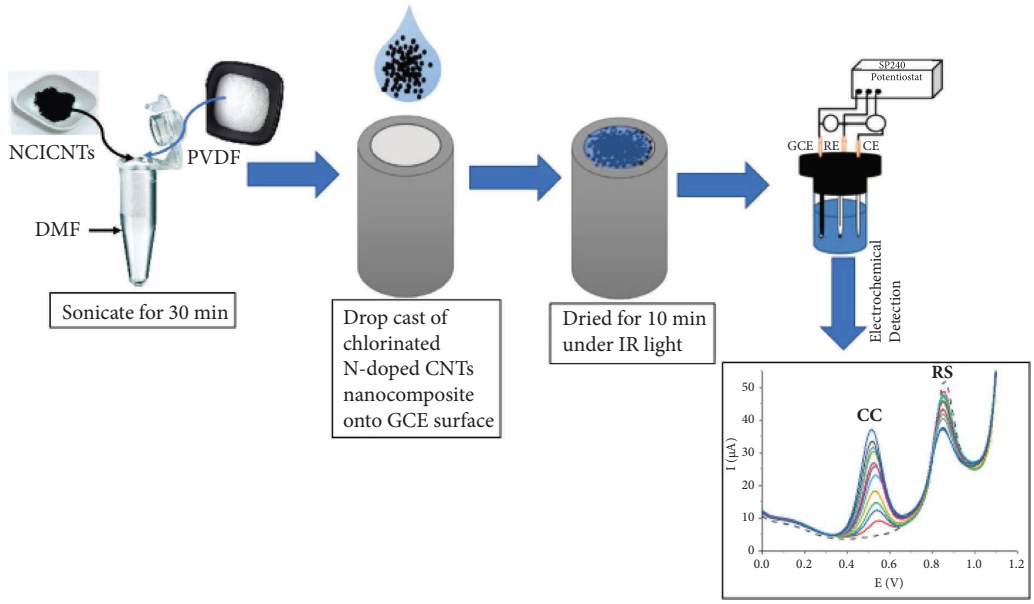

Scheme 1: Illustration of the electrode preparation and electrochemical tests.

3. Results and Discussion

3.1. Structural and Morphological Studies. The morphological properties of the nanostructured materials prepared by varying the concentration of chlorine in the acetonitrile feed were evaluated using TEM and SEM. Figure 1(a) represents a TEM image taken from our previous study prepared by the addition of chlorine vapours into the CVD reactor that contained an iron-cobalt catalyst as substrate while using dichlorobenzene as a source of chlorine [38]. As it can be clearly seen from the figure, secondary carbon nanofibers (CNFs) were grown on the surface of the principal CNTs (Figure 1(a), circled parts), and the growth was thought to have emanated from defected tubes, and that the defects were created by chlorine [38]. In this study, the effect of chlorine concentration on the morphology and the growth of nitrogen-doped CNTs were therefore evaluated. Figures 1(b) and 1(c) present TEM images obtained when about 33.3 vol.% of dichlorobenzene was mixed with 66.7 vol.% of acetonitrile making the volume ratio to be 2 : 1 (CH_3CN : DCB). The average outer diameters (obtained using ImageJ) of the chlorinated nitrogen-doped CNTs have increased tremendously (~115 nm, Supplementary Figure S1b, Table 1) when compared to the diameter of CNTs prepared from pure DCB which was about 33 nm [38]. Some of the CNTs appeared compartmented which is evidence of nitrogen doping or could also have emanated from the morphology of the metal catalyst that was used as a substrate [42] (Figure 1(b)), and some intratubular segmentations can also be observed which appeared to also be responsible for their increased diameters. Metal nanoparticles encapsulated inside the CNTs were also observed in some CNTs (Figure 1(b) circled). The corresponding SEM images are presented in Figure 1(d) and Supplementary Figure S1a, and they showed that the CNTs were entangled.

Nanostructures generated from the solution mixtures containing an increased concentration of DCB (66.7 vol.%) and reduced concentration of CH_3CN (33.3 vol.%) appeared much thinner, with notable bamboo-compartmented structures, and had rough surfaces, whereas some were hollow and others bent (Figure 2(a)). All these structural features showed that these materials were highly defected. Their average outer diameters (~57 nm) were greatly reduced in comparison to those generated at low concentrations of DCB (33.3 vol.%) (Table 1, Supplementary Figures S1c and S1d). Nitrogen-doped CNTs of various sizes and morphologies were obtained for nanostructures generated at high concentrations of DCB (66.7 vol.%), which showed that the selectivity was lost at this concentration (Figure 2(b)). The observed increase in the diameter of the CNTs with the addition of chlorine during the synthesis of chlorinated N-doped CNTs may imply that the catalyst particle increased in size during the CVD process.

Note that the CNT diameter increased tremendously at low chlorine concentrations, due to an interaction between iron and Cl_2, which modulates the iron-cobalt catalyst and promotes the aggregation of catalyst particles by thermal diffusion [43]. Therefore, we can conclude that at low chlorine concentration, the size of the catalyst and the diameter of the CNTs increased because of chlorine addition. However, when the concentration of chlorine was doubled, the diameter of the NCNTs decreased tremendously to almost half of that produced at low concentrations. These phenomena can be explained to arise because of the counteracting of the thermal diffusion of iron by iron etching with chlorine [43]. In our previous study [39], the addition of about 80% of chlorine to the CH_3CN feed resulted in the production of mixtures of open-ended CNTs, closed-ended entangled CNTs, and carbon nanospheres, and the yield only increased by 0.18 g from the original catalyst mass. A yellowish-brownish liquid was also observed inside

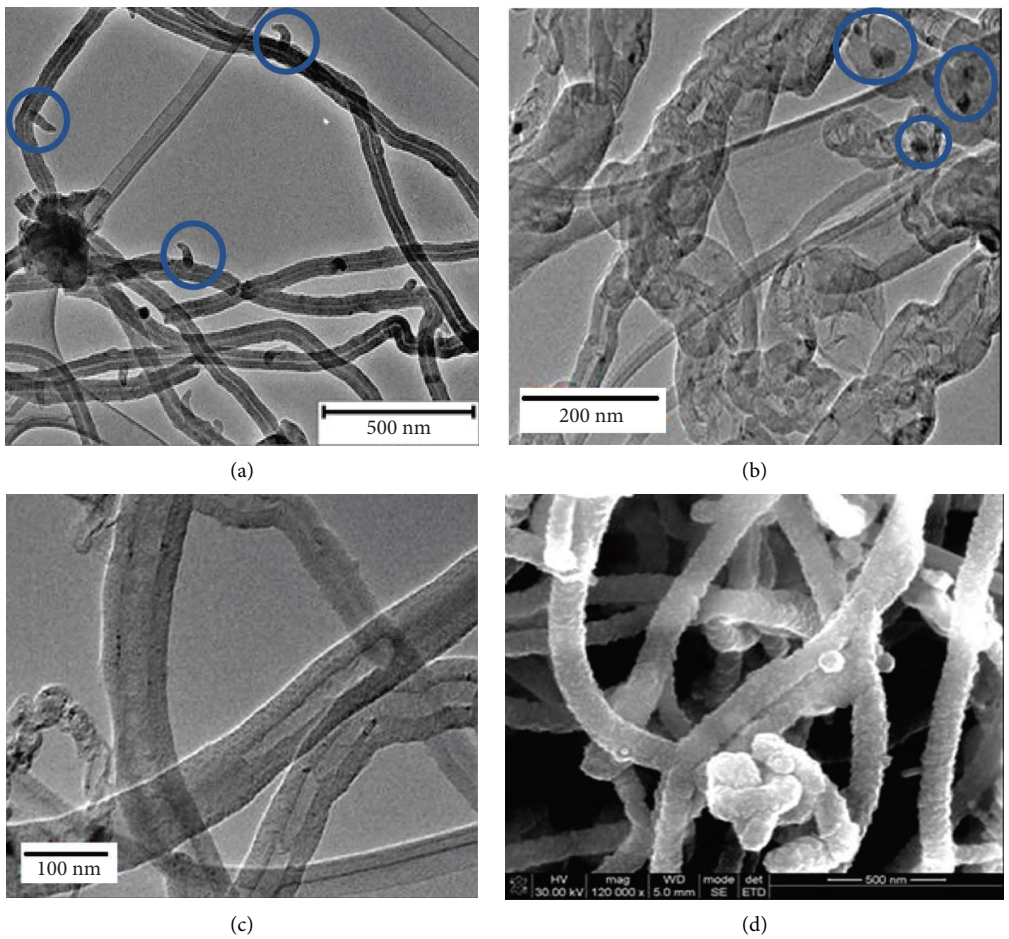

(a) (b) (c) (d)

Figure 1: TEM images of purified CNTs generated from (a) pure DCB, (b, c) mixture of CH_3CN : DCB (2 : 1 vol.%) obtained using a bubbling CVD method, and (d) the corresponding SEM image obtained from feed mixture.

Table 1: Diameter analysis of purified NCNTs generated from CH_3CN feeds containing various concentrations of DCB.

CH_3CN : DCB volume ratio	Outer diameter range (nm)	Average outer diameter (nm)	Average inner diameter (nm)	Number of structures counted	Reagent volume used (mL)
66.7 : 33.3 (2 : 1)	75–176	115 ± 34.2	22	>300	4
33.3 : 66.7 (1 : 2)	30–90	64 ± 15.5	14	>300	3

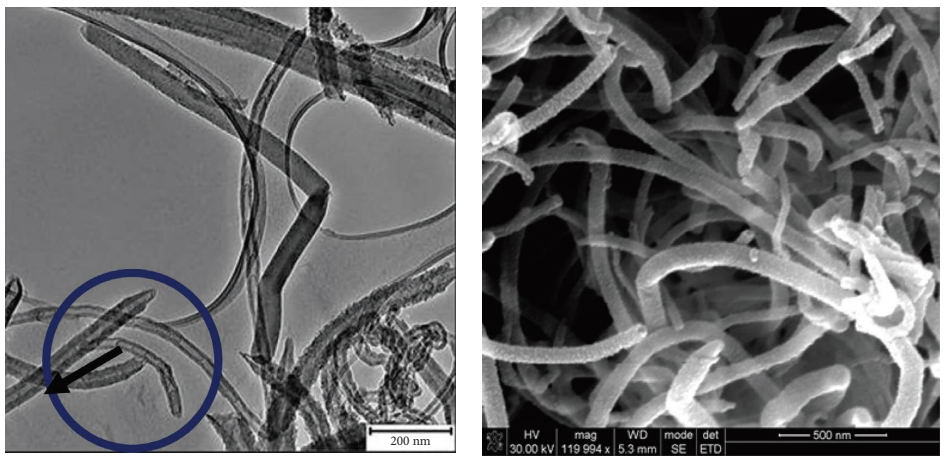

(a) (b)

Figure 2: TEM (a) and SEM (b) images generated from a mixture of CH_3CN : DCB (1 : 2 vol.%).

the quartz tube downstream, confirming that iron was etched by chlorine at high chlorine concentrations. In conclusion, we can say it is important to control the concentration of chlorine added to the acetonitrile feed to avoid etching of the iron nanoparticles because catalyst etching advances as the chlorine concentration increases.

Thermal gravimetric studies were conducted for NCNTs synthesized in the presence of various concentrations of chlorine to study their decomposition and oxidation resistance. TGA curves are presented in Figure 3. We observed a sharp weight decrease at ~500°C in the TGA spectra of N-doped samples produced at high concentrations of chlorine (1 : 2 ratio), which indicates that the chlorinated NCNTs are likely to react and also contain uniformly distributed defects along their entire surface (Figures 4(a) and 4(b)). For chlorinated NCNTs generated from a 2 : 1 volume ratio feed, the initial degradation was observed at higher temperatures of 550°C to 850°C which showed that the materials were less disordered (Figure 4(a)). The higher initial degradation temperatures in these materials could be because of the larger diameter CNTs produced in this feed (Figure 4(a)). Loss of water was also observed by the weight loss at around 80°C for NCNTs (1 : 2). About 10% weight loss was also observed at temperatures below 500°C from NCNTs (1 : 2), and this was attributed to oxidation of amorphous carbon [44]. The observed DTGA curve was also broad, which could indicate the oxidation of various shaped nanomaterials at the 2 : 1 volume ratio (Figure 4(b)). TGA data also depicted that the weight loss was around 100% and 92.3% for chlorinated NCNTs generated from 1 : 2 and 2 : 1 solvent mixture, respectively (Supplementary Table S1). The remaining material observed from chlorinated NCNTs generated from 2 : 1 solvent mixture could be the catalyst residues. These catalyst particles were observed from the TEM images trapped inside the chlorinated NCNTs tubes (Figure 1(b), circled parts) and could not be removed during acid treatment due to the thick walls of the chlorinated NCNTs whereas with the chlorinated NCNTs generated from 1 : 2 solvent mixture, all the catalyst particles were removed by acid treatment, which was made easy by their thin walls, and also, most of the catalyst nanoparticles were etched by large amounts of chlorine that were added during synthesis. Supplementary Figure S2 presents TEM images of pristine NCNTs (1 : 2) and NCNTs (2 : 1) before purification with acid and catalyst particles can be seen on top of the CNTs. The absence of the catalyst residual mass in the NCNTs (1 : 2) could also be attributed to the purifying property of chlorine as literature has shown that chlorine can act as a purifying agent [45]. It was also observed from the TGA curves that the oxidation resistance of the nanotubes decreased as the chlorine concentration in the feed increased as a result of increased density of defects and wall reactivity due to the incorporation of N within the carbon crystal (Figure 3(a)).

The structural disorder of the two chlorinated NCNT materials was compared using Raman spectroscopy. Figure 4 presents representative spectra generated from 2 : 1 and 1 : 2 CH_3CN : DCB volume ratios. Evaluation of the I_D/I_G ratio revealed that chlorinated N-doped CNTs generated from 1 : 2 CH_3CN : DCB feed ratio were highly defected with ratios of ~1.0, showing that an increase in chlorine concentration significantly increased the level of disorder in the chlorinated NCNTs, in comparison to I_D/I_G ratio of ~0.63 obtained for chlorinated N-doped CNTs generated from 2 : 1 volume ratios. Similar observations were made from the TEM analysis, as the chlorinated NCNTs walls had rough surfaces or appeared corrugated with an increase in DCB concentration. The absence of the 2D peak on NCNTs (1 : 2) materials also supports the observation that these materials were less graphitic. This could again be correlated to the etching of iron by chlorine which occurred at high chlorine concentrations. It appears that highly crystalline materials were generated at low levels of chlorine than at high levels of chlorine. At low levels of chlorine, there is increased diffusivity of carbon in the iron catalyst, which enables carbon to bond to more favourable sites in the CNT crystal, thus improving their crystallinity [43].

XPS analysis of materials generated in the presence of pure DCB as reported in our previous study did not show any nitrogen content, and the amount of chlorine was also very minimal [46]. This was expected since CNTs were synthesized by bubbling nitrogen gas and acetylene gas through dichlorobenzene solvent at room temperature, and the chlorine vapours generated could not have been sufficient to functionalize on the surface of the CNTs. However, the Cl2p peak could still be deconvoluted into two peaks at 199 and 200.1 eV, and these were associated with chloride ion and C-Cl bonds [46]. The Cl $2p_{1/2}/2p_{3/2}$ ratios were below ca.1.6, which indicates that only ionic chloride was present [46]. EDS analysis showed that about 0.12 wt.% of chlorine was present in this sample. The survey XPS spectrum of both chlorinated NCNTs revealed the presence of C1s, O1s, and N1s peaks (Supplementary Figure S3). A Cl2p peak was not observed in the chlorinated N-doped CNTs. The lack of incorporation of chlorine into this material could be a result of the high synthesis temperature of 800°C utilized during the synthesis, as opposed to the synthesis temperature of 700°C that was used for the synthesis of chlorinated CNTs from pure DCB. In our previous study, the effect of temperature on the morphology of chlorinated CNTs using DCB as a source of chlorine was investigated [38]. CNTs generated at a reaction temperature of 800°C did not present any secondary CNF growth on the surface of the CNTs, and the materials were highly graphitic with very low I_D/I_G values of less than 1 [47]. The highly graphitic nature of the material was attributed to the purification property of chlorine. It was suggested that at high synthesis temperatures, chlorine molecules were generated at a quick rate which resulted in them being at a very close proximity to each other, after which they reacted to form Cl_2 molecules which acted as purifying agents and were hence not involved in defect creation, but they simply escaped through the trap after purifying the material. Both materials revealed the main peak due to C1s, with a peak at ~283 eV representing the C-C sp^2, which was a typical graphitic carbon peak (Figures 5(a) and 5(b)). Three additional peaks were deconvoluted at 284, 286, and 289.0 eV assigned to the C-C sp^3, C-Cl/C-CN, and O=C-O bonding environments, respectively.

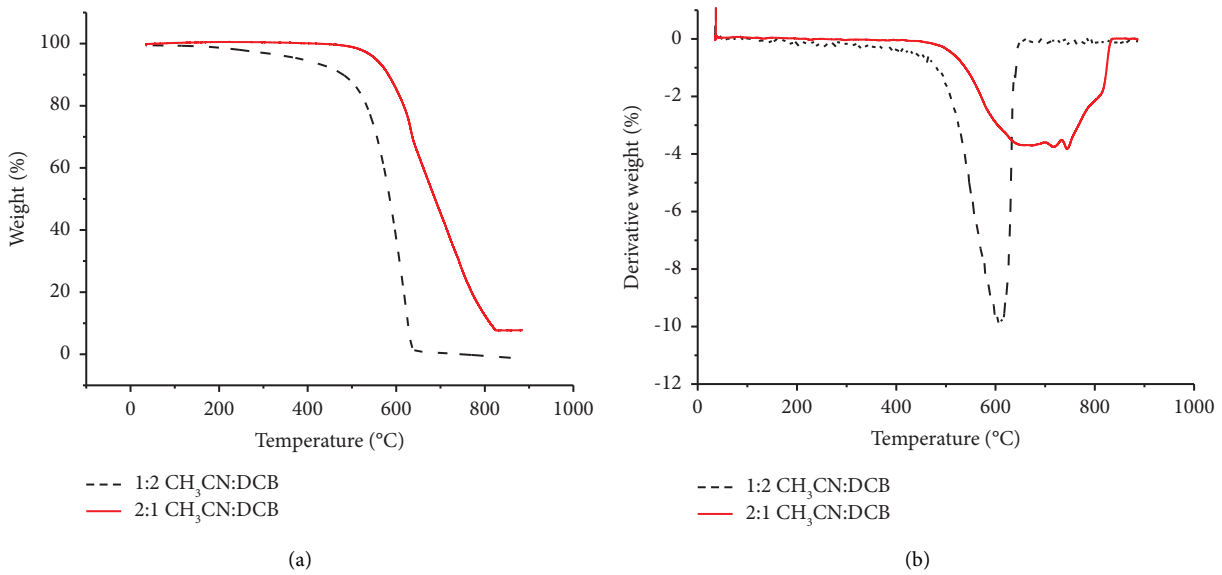

Figure 3: TGA (a) and derivative TGA (b) curves of purified chlorinated N-doped CNTs generated from solution mixtures of CH_3CN and DCB by various volume ratios.

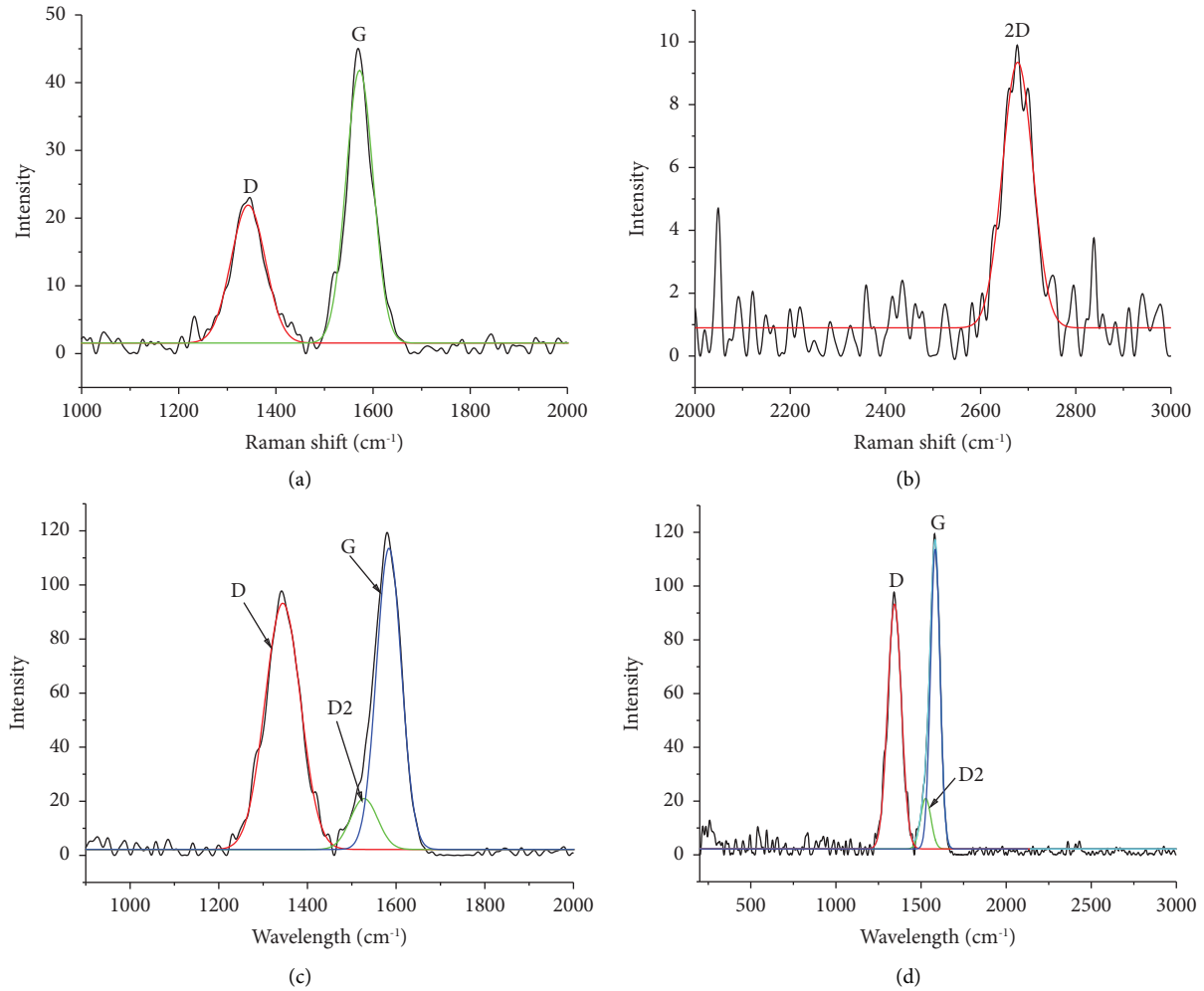

Figure 4: Deconvoluted Raman spectra of purified chlorinated N-doped CNTs generated from a feed containing (a, b) 2 : 1 and (c, d) 1 : 2 vol.% CH_3CN : DCB reagent mixture.

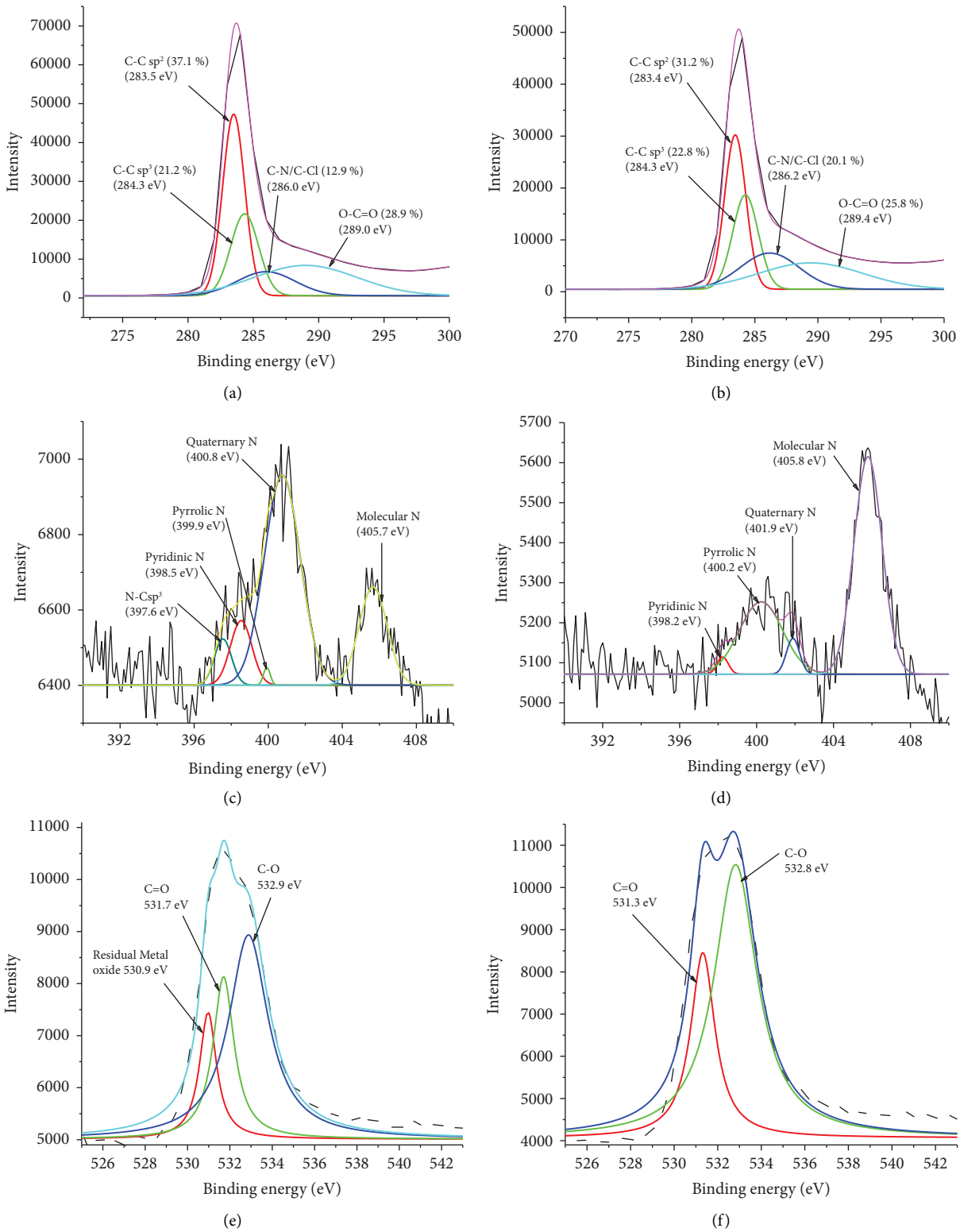

Figure 5: Deconvoluted C1s, N1s, and O1s XPS spectra of purified chlorinated N-doped CNTs generated from (a, c, e) 2 : 1 vol.% and (b, d, f) 1 : 2 vol.% of CH_3CN : DCB.

Chlorinated N-doped CNTs (2 : 1) produced at a low concentration of chlorine presented a smaller nitrogen content (0.84 at.%) in relation to chlorinated N-doped CNTs (1 : 2) produced at a high concentration of chlorine which had a nitrogen content of 1.29 at.%. These data correlate with the I_D/I_G ratio where the greatest amount of disorder was presented in NCNT (1 : 2). Literature has shown that increased nitrogen content leads to more crystalline defects in

the graphitic structure [48]. We also evaluated the dominating nitrogen species in chlorinated N-doped CNTs produced from the two feeds since it is known that the physicochemical and electrocatalytic properties of N-doped CNTs rely on the type of nitrogen bonding formed during synthesis and on the nitrogen content [49]. The deconvoluted N1s XPS spectra of chlorinated N-doped CNTs (2 : 1) generated from low concentrations of chlorine revealed that the quaternary nitrogen species was dominating in this material (Figure 5(c)). These results suggest a more homogeneous distribution of nitrogen species in the CNT crystal. Graphitic N forms by merging N atoms into the defect region of graphene, resulting in a graphene with fewer defects [50]. The deconvoluted N1s XPS spectra of chlorinated N-doped CNTs (1 : 2) generated from high concentrations of chlorine showed that the molecular and pyrrolic N species were dominating (Figure 5(d)). The pyrrolic nitrogen is known as a substitutional nitrogen, and it is part of a five-membered ring and is sp^3 hybridized. Pyrrolic arrangements can induce capped and disordered structures creating bamboo-shaped compartments, and they can also be located at the edges [51, 52].

XPS corroborated with Raman data where higher nitrogen content in chlorinated N-doped CNTs (1 : 2) was attributed to the higher I_D/I_G ratio (1.0), showing a less graphitic structure with more defects and more prone to nitrogen heteroatoms [53].

We also analysed the O1s peak, and three peaks appearing at 530.9, 531.7, and 532.9 eV were deconvoluted for chlorinated N-doped CNTs (2 : 1) generated at low chlorine concentration, which was attributed to residual metal oxide, C=O and C-O oxygen functional groups, respectively (Figure 5(e)). However, only the C=O and C-O oxygen functional group peaks were observed for chlorinated N-doped CNTs (1 : 2) generated at high chlorine concentration (Figure 5(f)). The presence of a residual metal oxide peak in materials generated from low chlorine concentrations confirms metal encapsulation in these chlorinated N-doped CNTs (2 : 1) as observed from TEM and TGA studies.

3.2. Electrochemical Behaviour of CC and RS of NClCNTs (2 : 1)/GCE. The electrochemical behaviour of CC and RS was first studied at different electrodes in a 0.1 M PBS of pH = 7.2. The corresponding cyclic voltammetry (CV) curves are presented in Figure 6. Catechol exhibited a quasi-reversible redox reaction at a bare GCE and GCE modified with NCNTs (1 : 2) with ΔE_p of ~200 mV (Figure 6(a)). The oxidation peak obtained at bare GCE had an exceptionally low resolution and intensity, indicating that CC cannot be quantified on a bare GCE. The oxidation and reduction peaks were less defined, but their intensities increased when using GCE modified with NCNTs (1 : 2), and this was attributed to the instability of their oxidizing and reducing intermediates [49]. Quasi-reversibility was maintained when using a GCE modified with NCNTs (2 : 1), even though ΔE_p slightly decreased to 184 mV. The obtained CC oxidation and reduction peaks were well-defined and highly intense when detected using GCE modified with NCNTs (2 : 1). These results indicated that NCNT films generated from a mixture containing 2 : 1 (CH_3CN : DCB) ratio can accelerate electron transfer. Similar electrochemical activity was observed for solutions containing RS as an analyte. However, RS exhibited an irreversible oxidation peak at potentials of ~0.75 V (Figure 6(b)). The RS peak was more defined and enhanced when using the GCE modified with NCNTs (2 : 1). Enhanced anodic peak currents were observed during the detection of acetaminophen using DPV when using GCE modified with larger diameter chlorinated N-doped CNTs produced at high temperature (850°C) as compared to modification with smaller diameter CNTs generated at 750°C [54]. The increased electrochemical performance of NCNTs (2 : 1) modified electrode was also attributed to the greatest graphitization observed in this material as evidenced by XPS and a low I_D/I_G Raman value compared to high values obtained with NCNTs (1 : 2).

3.2.1. Effect of pH. We then evaluated the effect of pH on the oxidation peak of CC and RS in 0.1 M PBS using a GCE modified with larger diameter NCNTs (2 : 1) material. The electrochemical response of the phenolic compounds was seen to be influenced by the pH since it affected the involvement of proton transference in the redox process [55]. Figures 7(a) and 7(b) show the effect of pH on anodic peak current and peak potential of CC (0.2 mM) and RS (0.8 mM) analysed using NCNTs (2 : 1)/GCE. The anodic peak current of CC decreased with an increase in pH from pH 2–4 and then increased to almost the same current as that measured from pH 2 to 5, and another large decrease was observed at pH 6–8. pH of 2 was, however, taken as an optimum based on the well-defined anodic DPV peak that was obtained compared to an anodic peak obtained at pH 5 (Figure 7(c)). In the case of RS, a decrease in pH was also observed at pH 2–6, with a slight increase observed at pH 7 but still lower than that obtained at pH 2. As a result, pH 2 was also taken as the optimum pH condition to be used for the simultaneous detection of CC and RS. This behaviour is acceptable because of the pKa of each molecule (CC = 9.4 and RS = 10.0), which means that with increasing pH, the molecules acquire a negative charge as they approach the pH in which they are protonated [56]. In our study, we have stipulated that chlorine-containing functional groups and nitrogen atoms on chlorinated N-doped CNTs surface may become deprotonated and possess negative charges at higher pH values [57]. As such, dihydroxybenzene isomers also become readily available to be deprotonated to form anions with increasing pH values [49]. The potential of the oxidation peak E_{pa} at CC and RS shifted negatively with an increase in pH, indicating that the protons were directly involved in the redox process [58]. However, a deviation is observed when the pH changed from 4 to 5 where a shift in the peak potential to more positive potential was observed. A positive shift in potential from pH 4 to 5 could imply that the quasi-reversible electrochemical process is shifted towards the irreversible process [59]. And the fact that the current intensity of the peak potential at pH 5 is equal to the current

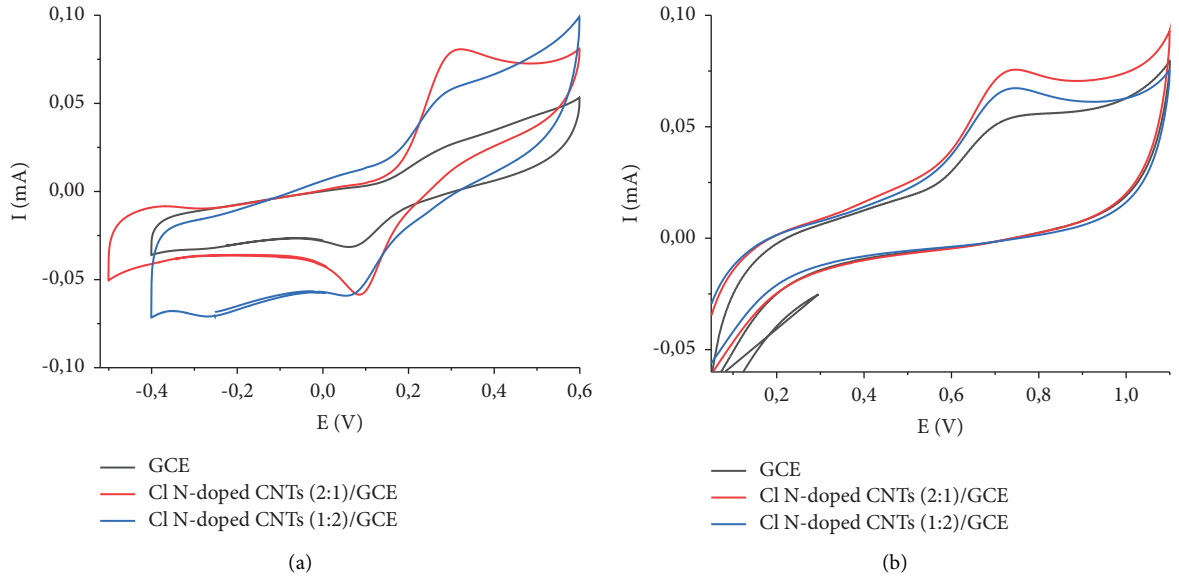

Figure 6: Cyclic voltammogram recorded at a bare GCE, chlorinated N-doped CNTs (1 : 2)/GCE, and chlorinated N-doped CNTs (2 : 1)/GCE at a scan rate of 50 mVs^{-1} in 0.1 M PBS of pH 7.2 containing (a) 0.5 mM CC and (b) 0.4 mM RS.

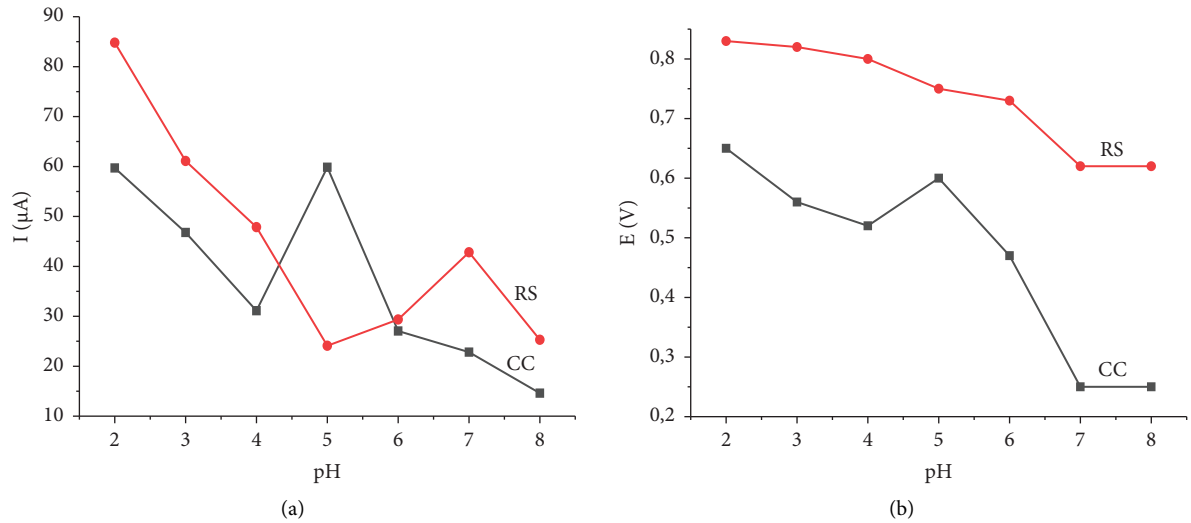

Figure 7: Continued.

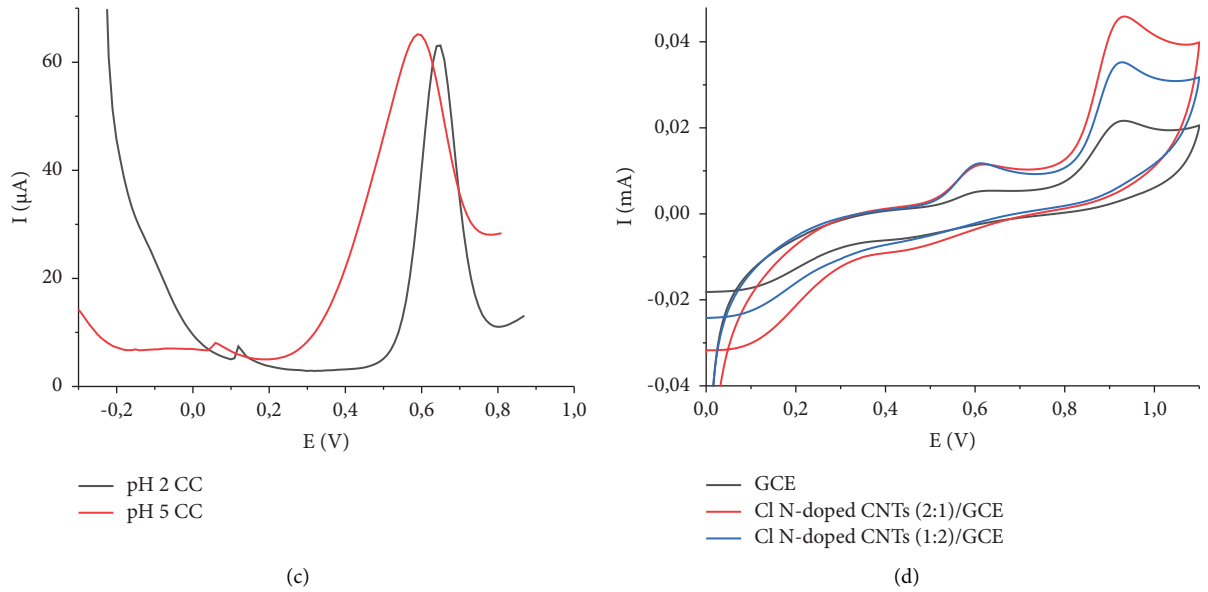

Figure 7: (a and b) Effect of pH on the anodic peak current and peak potential of CC (0.2 mM) and RS (0.8 mM) in 0.1 M PBS at GCE/chlorinated N-doped CNTs (2 : 1), (c) comparison of DPV curves obtained using pH 2 and 5 buffer solutions in the presence of 0.2 mM CC, and (d) cyclic voltammogram recorded at bare GCE, chlorinated N-doped CNTs (1 : 2)/GCE, chlorinated N-doped CNTs (2 : 1)/GCE at a scan rate of 50 mVs^{-1} in 0.1 M PBS of pH 2 containing 0.2 mM CC and 0.2 mM RS.

intensity at pH 2 can also clarify that the processes taking place at these two pHs must be similar; hence, it is expected for them to be oxidized at almost the same potential.

CV curves obtained for solutions containing 0.2 mM CC and RS in 0.1 M PBS at pH 2 were then used to evaluate their behaviour at this pH. The obtained CV curves measured in the presence of both CC and RS in PBS buffer pH 2 over NCNTs (2 : 1)/GCE revealed two well-separated oxidation peaks at ~0.58 V for CC and ~0.86 V for RS (Figure 7(d)). As a result, a PBS buffer solution of pH 2 was used for the simultaneous detection of CC and RS to obtain the optimal sensitivity and selectivity.

3.2.2. Effect of Scan Rate. A NCNTs (2 : 1)/GCE sensor was used for the simultaneous detection of CC and RS in 0.1 M PBS of pH 2. DPV curves showed well-separated peaks at voltages of +0.58 V for CC and +0.86 V for RS (Figure 8(a)). The electrooxidation process of CC and RS was then studied by CV varying the scan rates from 10 to 55 mVs^{-1} using 0.2 mM CC and RS in 0.1 M PBS (pH 2) (Figure 8(b)). The redox peak currents of CC ($r = 0.9958$ (I_{pa}) and 0.9754 (I_{pc})) and RS ($r = 0.9914$) increased with an increase in scan rate (Figure 8(b)). There was a linear relationship between the square root of the scan rate and the oxidation peak current, which confirmed that the electrooxidation process of CC and RS on NCNTs (2 : 1)/GCE is regulated by the diffusion-controlled electrochemical process (Figures 8(c) and 8(d)) [60]. A shift in the oxidation peak potentials to higher potentials with increasing scan rate was attributed to a tendency of the redox process to shift from quasi-reversible to irreversible [61]. This is also because the concentration of the analyte at the surface of the electrode does not vary at high scan rates since the electron transfer rate constant becomes slow with fast scans since more extreme potentials are needed to induce electron transfer [62].

3.2.3. Simultaneous Determinations of CC and RS. The simultaneous and quantitative determination of the two dihydroxybenzene isomers was carried out by DPV of NCNTs (2 : 1)/GCE when the concentration of one isomer changed and of one remained constant (Figure 9). Figures 9(a) and 9(b) show DPV curves of 0.2 mM RS with different concentrations of CC and 0.2 mM CC with different concentrations of RS. The peak current of CC increased linearly with an increase in CC concentration from 0.1 to 1.2 mM ($R^2 = 0.9930$), and the peak current of RS also increased linearly with an increase in RS concentration from 0.05 to 1.2 mM ($R^2 = 0.9986$) (Figure 9(c)). The limits of detection for CC and RS were estimated to be 0.059 μM and 0.034 μM (3S/M), respectively. In addition to the current limit of detection and wider linear range, the proposed material possesses the virtue of a simple electrode preparation process and avoids the time-consuming electrode modification process utilized in other materials. These results suggest that CC and RS can be selectively and simultaneously determined in NCNTs (2 : 1)/GCE in their binary mixtures. The excellent analytical performance may be attributed to the morphology of NCNTs (2 : 1) and the synergistic effect of chlorine on the N-doping effect and its enhanced defect creation which greatly increased the electrocatalytic active area and active sites, consequently promoting the electron transfer reaction of dihydroxybenzene isomers on the electrode surface. The limits of detection obtained in the current work were also compared to those obtained for detection of catechol and resorcinol, using

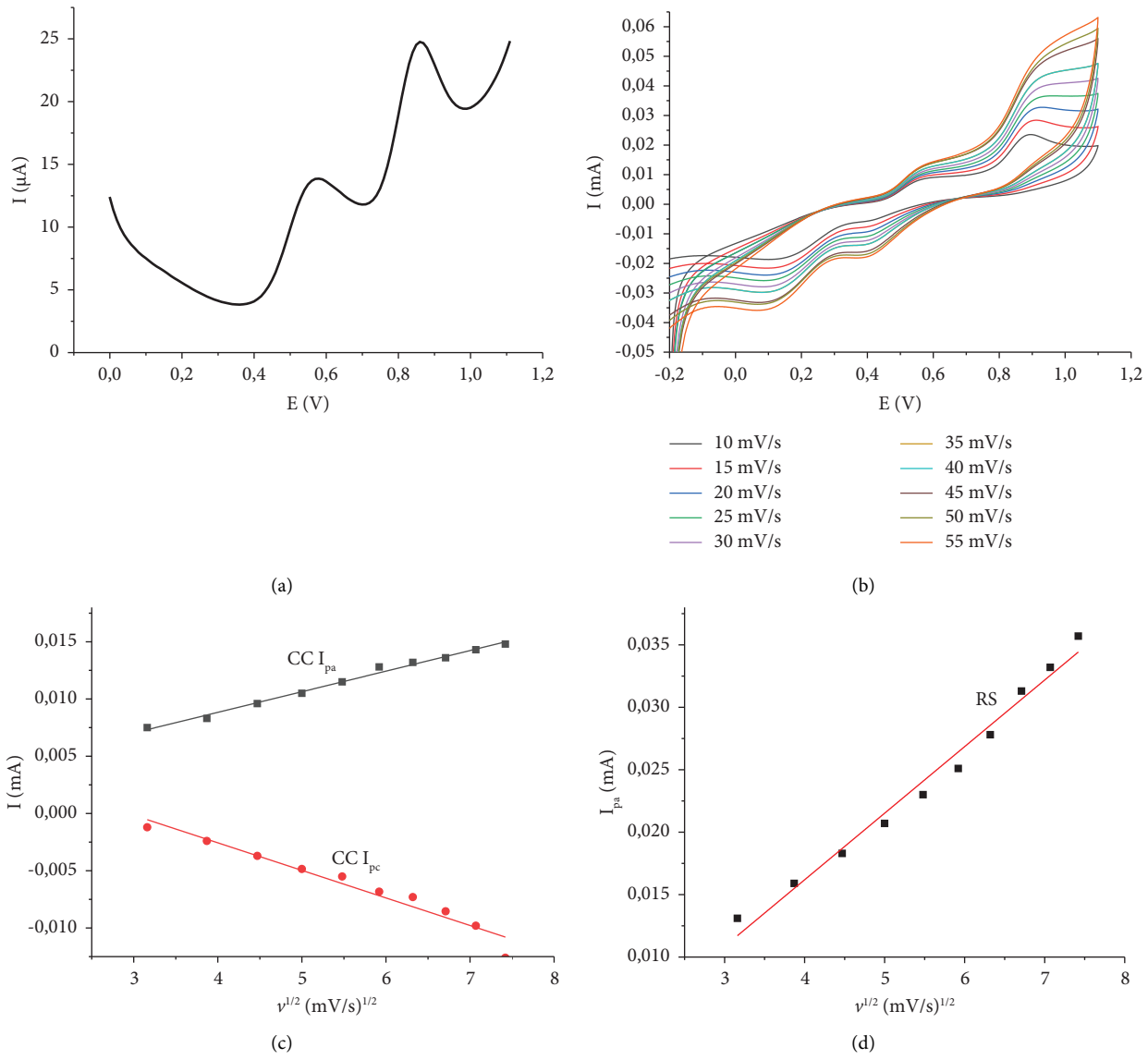

Figure 8: (a) DPV curve for simultaneous detection of 0.8 mM CC and RS, (b) effect of scan rate on the redox behaviour of the mixture of 0.2 mM of CC and RS in 0.1 M PBS (pH 2) of NCNTs (2 : 1)/GCE, and (c, d) plots of peak current versus square root of scan rates for CC and RS.

other types of modified CNTs, and they were quite comparable proving that the current sensor can be used for detection of this analytes in water (Table 2).

To evaluate the repeatability of GCE modified with NCNTs (2 : 1), the peak currents of ten successive measurements of DPV in the binary solution mixture of 0.2 mM RS and 0.3 mM CC were determined. The repeatability of the modified sensor was determined in the same electroanalytical solution. There was no difference in the peak current signals for both CC and RS across all measurements (Supplementary Figure S4). This is an indication that the modified sensor has excellent repeatability. The relative standard deviations (RSDs) of 0.72% and 3.14% were obtained for RS and CC, respectively.

The stability of the NCNTs (2 : 1)/GCE was also tested. In this case, the NCNTs (2 : 1)/GCE was covered and stored at room temperature for 2 weeks. The stability was calculated by comparing the percentage (%) of current retention to the initial response. The percentage retention of CC and RS reached 87% and 94% of the initial value, respectively, indicating high stability.

3.2.4. Interference Studies. To evaluate the selectivity of the NCNTs (2 : 1)/GCE, the influence of some possible interferents on the determination of 0.4 mM CC and RS was studied (Figure 10). It is considered to have no interference when the current variation caused by interferents is less than 5%. It was found that a 200-fold concentration of Cl^-, NO_3^-, K^+, Ca^{2+}, Mg^{2+}, Zn^{2+}, and Fe^{3+} had no obvious interference to the determination of CC and RS, with the maximum signal change of 5% observed (Figure 10). When Cu^{2+} was added as an interference ion, an additional peak was observed at around 0.19 V, which had almost the same intensity as that of CC and RS (Supplementary Figure S5). The CC peak and RS

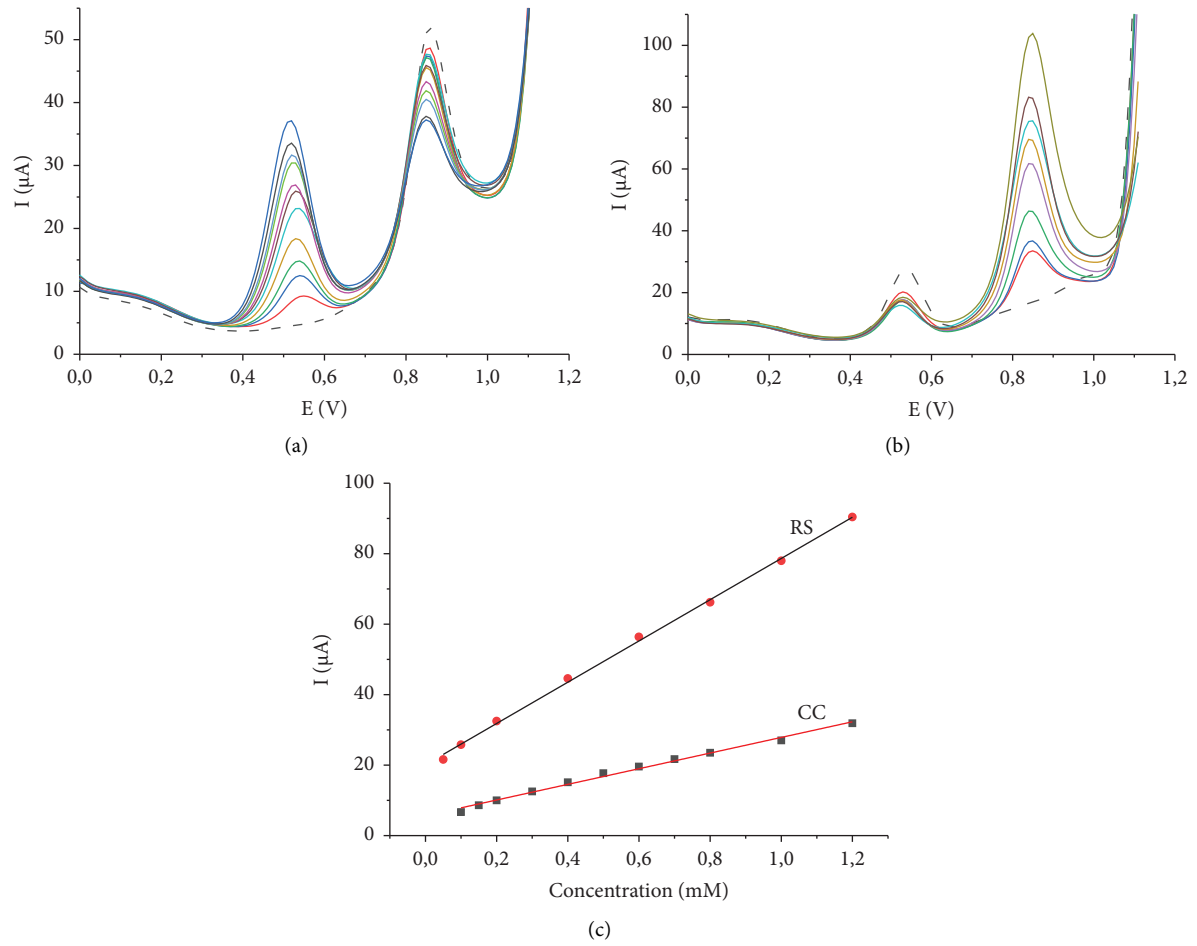

Figure 9: (a) DPV curves of different concentrations of CC (0, 0.1, 0.15, 0.2, 0.3, 0.4, 0.5, 0.6, 0.7, 0.8, 1.0, 1.2 mM) in the presence of 0.2 mM RS using NCNTs (2 : 1)/GCE; (b) DPV curves of different concentrations of RS (0, 0.05, 0.1, 0.2, 0.4, 0.6, 0.8, 1.0, 1.2 mM) in the presence of 0.2 mM CC using NCNTs (2 : 1)/GCE; (c) the calibration plot shows oxidation peak currents as a function of CC and RS concentration.

Table 2: Comparison of the sensors prepared in this work for the detection of CC and RS with other heteroatom-doped carbon nanomaterials modified GCE.

Sensor	Method	Linear range (mM)		LOD (μM)		Ref
		CC	RS	CC	RS	
O_2 plasma-treated CNTs	CV	0.001–1	—	0.60	—	[28]
Lac-F,N-CDs/GCE	*i-t*	0.012–0.450	—	0.014	—	[29]
Sm_2O_3/f-MWCNTs/GCE	DPV	0.0001–1.249	—	0.03		[31]
Poly-SA/MWCNTs/CPE	DPV	0.003–0.240	—	0.16		[32]
PS-PDEA-PS/C_{60}-MWCNTs/CPE	DPV	0.004–0.135	—	1.45		[33]
MWCNTs/p-DAN/GCE	DPV	0.000002–0.130	—	0.01		[34]
fMWCNTs/ZnO@ fMWCNTs/GCE	CV	0.010–0.200	—	0.027		[35]
SDS-modified graphenepaste electrode	CV	0.002–0.01	—	0.106	—	[37]
Fe-Cu-based MOF/rGO	DPV	0.0001–0.800	0.006–0.720	0.016	0.02	[11]
NCNTs (2 : 1)/GCE	DPV	0.1–1.2	0.05–1.2	0.059	0.034	This work

peak in the Cu^{2+} solution were also reduced, but Cu^{2+} did not interfere much because it was observed at a different potential from our studied analytes. The observed reduction was 3 times for CC and by almost 2 times for RS. We can conclude not only that Cu^{2+} will cause interference if present at low concentrations but also that the electrode is capable of simultaneous detection of CC, RS, and Cu^{2+} ions in solution.

We also investigated the interference of hydroquinone (HQ) which is mostly present in water solutions together with CC and RS. DPV curve of HQ, CC, and RS alone in solution revealed that their oxidation peaks occurred at

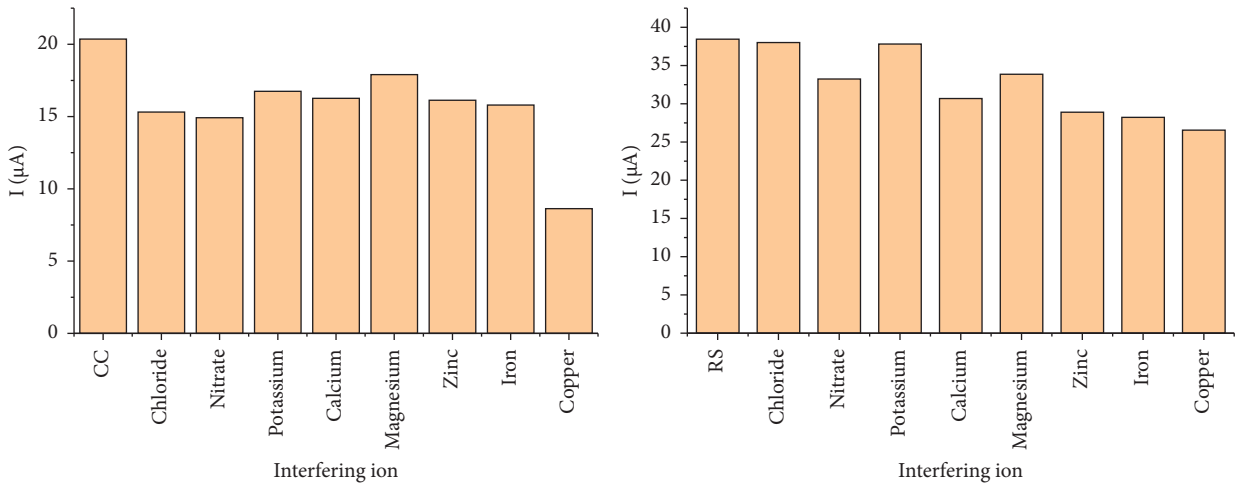

Figure 10: Bar chart of interfering ions for selectivity test of catechol and resorcinol sensor.

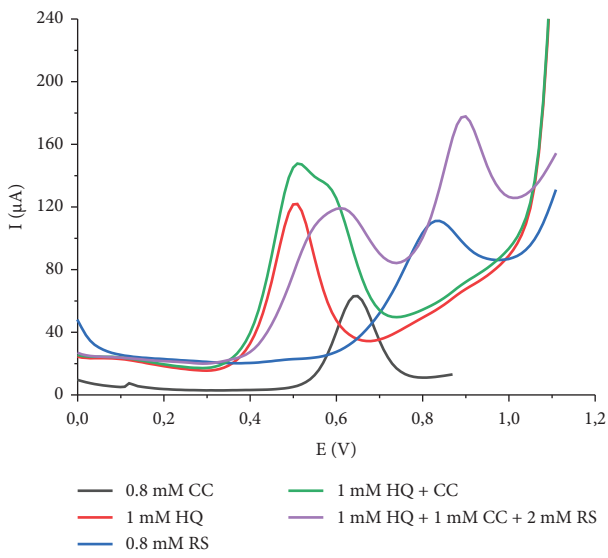

Figure 11: DPV curves of single 1 mM HQ, 0.8 mM CC, and 0.8 mM RS, and the binary mixture of 1 mM HQ and CC and their ternary mixture of 1 mM HQ, 1 mM CC, and 2 mM RS in 0.1 M PBS (pH 2) at GCE/NCNTs (2 : 1).

different potentials in 0.1 M PBS (pH 2), i.e., at 0.49, 0.65, and 0.86 V, respectively (Figure 11). However, when HQ was analysed together with CC in the same solution, the CC peak shifted to less positive potentials toward the potential where HQ is oxidized which resulted in their peaks overlapping, and a shoulder peak due to oxidation of CC could be observed at around 0.60 V (Figure 11). When all three dihydroxybenzene (HQ, CC and RS) analytes were mixed together in a ternary mixture, the HQ oxidation peak shifted to more positive potentials, resulting in it overlapping with the CC peak, which resulted in an observation of one broad peak at 0.60 V. However, an HQ peak at these concentrations could still be observed as a shoulder peak appearing at around 0.52 V (Figure 11).

The prepared sensor was also tested for its practical application as a detector for CC and RS in local tap water

Table 3: Recoveries of CC and RS in local tap water at NCNTs (2 : 1)/GCE.

Samples	Added (mM)		Found (mM)		Recovery (%)	
	CC	RS	CC	RS	CC	RS
Tap water 1	0.100	0.100	0.102	0.102	102	102
Tap water 2	0.100	0.100	0.0966	0.0997	96.6	99.7

samples using the standard addition method. In this method, tap water was diluted with a 0.1 M PBS (pH 2) in the ratio of 1 : 4. The recovery was performed by spiking the electrolyte solution with 0.100 mM CC and RS in both tap water samples. The percentage recoveries presented in Table 3 showed that the proposed sensor can successfully detect CC and RS in real water samples.

4. Conclusions

The role of chlorine on the morphology of nitrogen-doped carbon nanotubes was evaluated by the addition of various amounts of dichlorobenzene, and the resultant materials were coated onto the surface of a GCE for use as electrochemical detectors. Large diameter NCNTs were produced when the amount of chlorine in the feed was lower, and small diameter NCNTs were produced when the amount of chlorine in the feed was larger than that of the nitrogen source. Large diameter NCNTs coated electrode showed a wide linear range for studied concentrations and a low detection limit for the simultaneous detection of CC and RS which was attributed to them being highly graphitic. It was suggested that the addition of a low concentration of chlorine increased the carbon diffusivity in the catalyst, which resulted in the formation of compartmented larger diameter NCNTs, whereas when a large concentration of chlorine was added in the feed, etching of iron by chlorine occurred resulting in the formation of materials with smaller average diameters and was highly disordered. The low detection limits obtained that were comparable to those obtained for heteroatom-doped CNTs in the literature showed

that the chlorinated NCNTs (2 : 1) composite could be employed as an electrode material for the development of electrochemical sensors. The practical applicability of the detector was also shown by catechol and resorcinol detection in real water samples.

Data Availability

All data that support the findings of this study are included in the article (and additional data are provided in the supplementary files).

Conflicts of Interest

The authors declare that there are no conflicts of interest.

Acknowledgments

This work was supported by the National Research Foundation Thuthuka (Grant no. 138267) and Vaal University of Technology Research Grant. The authors acknowledge open access funding enabled and organized by SANLiC Gold. They would also like to acknowledge the following: Microscopy Microanalysis Unit at the University of the Witwatersrand for TEM and SEM analysis and Rhodes University for XPS analysis.

Supplementary Materials

Appendix A: *Supporting Information*. Supplementary data associated with this article can be found in the online version. Table S1: Decomposition temperatures and residual masses (determined by TGA and DTGA) of the unpurified and purified (P) chlorinated NCNTs generated from solutions containing different CH_3CN : DCB volume ratios. Figure S1: SEM images and diameter distributions curves of purified CNMs generated from CH_3CN feed containing 33.3 (a and b) and 66.7 (c and d) vol.% DCB by bubbling CVD method. Figure S2: TEM images of unpurified chlorinated NCNTs prepared in (a) 1 : 2 and 2 : 1 volume ratio of CH_3CN : DCB solvent mixture. Figure S3: Survey scan XPS spectra of NCNTs generated from various CH_3CN : DCB solvent mixtures. Figure S4: Bar chart of repeatability tests on NCNTs (2 : 1)/GCE in the presence of both CC and RS: (a) CC measurement and (b) RS measurement. Figure S5: DPV curves for detection of 0.4 mM RS and CC in 0.1 M PBS pH 2 over NCNTs (2 : 1)/GCE before (– solid lines) and after (. . .. dotted lines) addition of 80 mM Cu^{2+} as interference ion. (*Supplementary Materials*)

References

[1] S. M. Ghoreishi, M. Behpour, E. Hajisadeghian, and M. Golestaneh, "Voltammetric determination of resorcinol on the surface of a glassy carbon electrode modified with multi-walled carbon nanotube," *Arabian Journal of Chemistry*, vol. 9, pp. S1563–S1568, 2016.

[2] S. Palanisamy, C. Karuppiah, S. Chen et al., "Selective and simultaneous determination of dihydroxybenzene isomers based on green synthesized gold nanoparticles decorated reduced graphene oxide," *Electroanalysis*, vol. 27, no. 5, pp. 1144–1151, 2015.

[3] J. M. Harnly, S. Bhagwat, and L.-Z. Lin, "Profiling methods for the determination of phenolic compounds in foods and dietary supplements," *Analytical and Bioanalytical Chemistry*, vol. 389, no. 1, pp. 47–61, 2007.

[4] M. Govindhan, T. Lafleur, B. R. Adhikari, and A. Chen, "Electrochemical sensor based on carbon nanotubes for the simultaneous detection of phenolic pollutants," *Electroanalysis*, vol. 27, no. 4, pp. 902–909, 2015.

[5] F. J. Enguita and A. L. Leitao, "Hydroquinone: environmental pollution, toxicity, and microbial answers," *BioMed Research International*, vol. 2013, Article ID 542168, 14 pages, 2013.

[6] J. Huang, K. Huang, and C. Yan, "Application of an easily water-compatible hyper crosslinked polymeric adsorbent for efficient removal of catechol and resorcinol in aqueous solution," *Journal of Hazardous Materials*, vol. 167, no. 1-3, pp. 69–74, 2009.

[7] Q. Liao, J. Sun, and L. Gao, "The adsorption of resorcinol from water using multi-walled carbon nanotubes," *Colloids and Surfaces A: Physicochemical and Engineering Aspects*, vol. 312, no. 2-3, pp. 160–165, 2008.

[8] M. Arago, C. Arino, A. Dago, J. M. Diaz-Cruz, and M. Esteban, "Simultaneous determination of hydroquinone, catechol and resorcinol by voltammetry using graphene screen-printed electrodes and partial least squares calibration," *Talanta*, vol. 160, pp. 138–143, 2016.

[9] M. Zhang, J. Ye, P. Fang, Z. Zhang, C. Wang, and G. Wu, "Facile electrochemical preparation of NaOH nanorods on glassy carbon electrode for ultrasensitive and simultaneous sensing of hydroquinone, catechol and resorcinol," *Electrochimica Acta*, vol. 317, pp. 618–627, 2019.

[10] F. Garkani Nejad, H. Beitollahi, and I. Sheikhshoaie, "Graphene oxide-PAMAM nanocomposite and ionic liquid modified carbon paste electrode: an efficient electrochemical sensor for simultaneous determination of catechol and resorcinol," *Diagnostics*, vol. 13, no. 4, p. 632, 2023.

[11] K. D. Kıranşan and E. Topcu, "Graphene paper with sharp-edged nanorods of Fe-CuMOF as an excellent electrode for the simultaneous detection of catechol and resorcinol," *Electroanalysis*, vol. 31, no. 12, pp. 2518–2529, 2019.

[12] T. Sunil Kumar Naik and B. F. Kumara Swamy, "Pre-treated glassy carbon electrode sensor for catechol: a voltammetric study," *Journal of Electroanalytical Chemistry*, vol. 826, pp. 23–28, 2018.

[13] N. Maleki, S. Kashanian, E. Maleki, and M. Nazari, "A novel enzyme-based biosensor for catechol detection in water samples using artificial neural network," *Biochemical Engineering Journal*, vol. 128, pp. 1–11, 2017.

[14] B. S. Lynch, E. S. Delzell, and D. H. Bechtel, "Toxicology review and risk assessment of resorcinol: thyroid effects," *Regulatory Toxicology and Pharmacology*, vol. 36, no. 2, pp. 198–210, 2002.

[15] J. C. Prager, *Environmental Contaminant Reference Data Book*, Vol. 3, Van Nostrand Reinhold, New York, NY, USA, 1997.

[16] R. Raff and B. V. Etlling, *Kirk-Othmer Encyclopedia of Chemical Technology,*Vol. 11, Wiley-Interscience, New York, NY, USA, 1966.

[17] A. Kumar, S. Kumar, and S. Kumar, "Biodegradation kinetics of phenol and catechol using Pseudomonas putida MTCC 1194," *Biochemical Engineering Journal*, vol. 22, no. 2, pp. 151–159, 2005.

[18] R. Subramanyam and I. M. Mishra, "Biodegradation of catechol (2-hydroxy phenol) bearing wastewater in an UASB reactor," *Chemosphere*, vol. 69, no. 5, pp. 816–824, 2007.

[19] A. A. Aghapour, G. Moussavi, and K. Yaghmaeian, "Biological degradation of catechol in wastewater using the sequencing continuous-inflow reactor (SCR)," *Journal of Environmental Health Science and Engineering*, vol. 11, no. 1, p. 3, 2013.

[20] Y. Liu, M. Gao, Z. Gu, Z. Luo, Y. Ye, and L. Lu, "Comparison between the removal of phenol and catechol by modified montmorillonite with two novel hydroxyl-containing gemini surfactants," *Journal of Hazardous Materials*, vol. 267, pp. 71–80, 2014.

[21] W. Lu, X. Wang, X. Wu et al., "Multi-template imprinted polymers for simultaneous selective solid-phase extraction of six phenolic compounds in water samples followed by determination using capillary electrophoresis," *Journal of Chromatography A*, vol. 1483, pp. 30–39, 2017.

[22] K. S. Abd-Alrassol and E. Q. Jasim, "Spectrophotometric determination of some phenolic compounds by formation of copper (II) complexes," *IOP Conference Series: Materials Science and Engineering*, vol. 571, no. 1, Article ID 012097, 2019.

[23] W. Xu, Y. Hu, M. Wu et al., "Determination of phenolic compounds in estuary water and sediment by solid-phase isotope dansylation coupled with liquid chromatography-high resolution mass spectrometry," *Analytical Methods*, vol. 13, no. 11, pp. 1404–1411, 2021.

[24] A. S. Ahammad, M. A. Ullah, M. M. Hoque et al., "Signal enhancement of hydroquinone and catechol on their simultaneous determination," *International Journal of Electrochemical Science*, vol. 12, no. 8, pp. 7570–7579, 2017.

[25] Y. Chen, X. Liu, S. Zhang et al., "Ultrasensitive and simultaneous detection of hydroquinone, catechol and resorcinol based on the electrochemical co-reduction prepared Au-Pd nanoflower/reduced graphene oxide nanocomposite," *Electrochimica Acta*, vol. 231, pp. 677–685, 2017.

[26] S. M. Abu Nayem, S. Shaheen Shah, N. Sultana, M. A. Aziz, and A. J. Saleh Ahammad, "Electrochemical sensing platforms of dihydroxybenzene: Part 1 – carbon nanotubes, graphene, and their derivatives," *Chemical Record*, vol. 21, no. 5, pp. 1039–1072, 2021.

[27] S. Chen, R. Huang, J. Yu, and X. Jiang, "Simultaneous voltammetric determination of hydroquinone and catechol by using a glassy carbon electrode modified with a ternary nanocomposite prepared from oxidized multiwalled carbon nanotubes, manganese dioxide and manganese ferrite," *Microchimica Acta*, vol. 186, no. 9, p. 643, 2019.

[28] S. G. Wang, Y. Q. Li, X. J. Zhao, J. H. Wang, J. J. Han, and T. Wang, "Electrochemical detection of catechol at integrated carbon nanotubes electrodes," *Diamond and Related Materials*, vol. 16, no. 2, pp. 248–252, 2007.

[29] L. Liu, S. Anwar, H. Ding et al., "Electrochemical sensor based on F,N-doped carbon dots decorated laccase for detection of catechol," *Journal of Electroanalytical Chemistry*, vol. 840, pp. 84–92, 2019.

[30] W. Shenggao, W. Tao, L. Yanqiong, Z. Xiujian, H. Jianjun, and W. Jianhua, "Plasma activation of integrated carbon nanotube electrodes for electrochemical detection of catechol," *Plasma Science and Technology*, vol. 9, no. 2, pp. 194–197, 2007.

[31] B. Mutharani, S. Sakthinathan, S.-M. Chen, T.-W. Chen, and T.-W. Chiu, "Preparation of samarium oxide nanoparticles decorated functionalized multiwall carbon nanotubes modified electrode for the electrochemical determination of catechol," *International Journal of Electrochemical Science*, vol. 13, pp. 6996–7007, 2018.

[32] Y. Liang, J. Li, and Y. Zhao, "Poly(sulfosalicylic acid)/multiwalled carbon nanotube modified electrode for the electrochemical detection of catechol," *International Journal of Electrochemical Science*, vol. 12, no. 10, pp. 9512–9522, 2017.

[33] C. Chen, P. Zhao, C. Li, Y. Xie, and J. Fei, "Highly sensitive temperature-responsive sensor based on PS-PDEA-PA/C_{60}-MWCNTs for reversible switch detection of catechol," *Electroanalysis*, vol. 31, no. 5, pp. 913–921, 2019.

[34] A. M. Abdel-Aziz, H. H. Hassan, A. A. Hassan, and I. H. A. Badr, "A sensitive and green method for determination of catechol using multi-walled carbon nanotubes/poly(1,5-diaminonaphthalene) composite film modified glassy carbon electrode," *Journal of the Electrochemical Society*, vol. 166, no. 15, pp. B1441–B1451, 2019.

[35] M. Hicham, A. Fethi, S. Ha, and B. Khaldoun, "Antifouling double layers of functionalized-multi-walled carbon nanotubes coated ZnO for sensitive and selective electrochemical detection of catechol," *Fullerenes, Nanotubes, and Carbon Nanostructures*, vol. 30, no. 3, pp. 334–347, 2022.

[36] H. Rao, Y. Liu, J. Zhong et al., "Gold nanoparticle/chitosan@N,S Co-doped multiwalled carbon nanotubes sensor: fabrication, characterization, and electrochemical detection of catechol and nitrite," *ACS Sustainable Chemistry and Engineering*, vol. 5, no. 11, pp. 10926–10939, 2017.

[37] J. G. Manjunatha, "A surfactant enhanced graphene paste electrode as an effective electrochemical sensor for the sensitive and simultaneous determination of catechol and resorcinol," *Chemical Data Collections*, vol. 25, Article ID 100331, 2020.

[38] W. K. Maboya, N. J. Coville, and S. D. Mhlanga, "One-step synthesis of carbon nanotubes with secondary growth of carbon nanofibers: effect of chlorine, synthesis time and temperature," *Materials Research Express*, vol. 6, no. 11, Article ID 115016, 2019.

[39] W. K. Maboya, N. J. Coville, and S. D. Mhlanga, "Fabrication of chlorine nitrogen co-doped carbon nanomaterials by an injection catalytic vapor deposition method," *Materials Research Express*, vol. 8, no. 1, Article ID 015007, 2021.

[40] S. D. Mhlanga, K. C. Mondal, R. Carter, M. J. Witcomb, and N. J. Coville, "The effect of synthesis parameters on the catalytic synthesis of multiwalled carbon nanotubes using Fe-Co/$CaCO_3$ catalysts," *South African Journal of Chemistry*, vol. 62, pp. 67–76, 2008.

[41] Z. N. Tetana, S. D. Mhlanga, G. Bepete, R. W. M. Krause, and N. J. Coville, "The synthesis of nitrogen-doped multiwalled carbon nanotubes using an Fe-Co/$CaCO_3$ catalyst," *South African Journal of Chemistry*, vol. 65, pp. 39–49, 2012.

[42] J.-W. Jang, "Direct curvature measurement of the compartments in bamboo-shaped multi-walled carbon nanotubes via scanning probe microscopy," *Scientific Reports*, vol. 11, no. 1, p. 701, 2021.

[43] T. Kinoshita, M. Karita, N. Chikyu, T. Nakano, and Y. Inoue, "Enhancement of catalytic activity by addition of chlorine in chemical vapor deposition growth of carbon nanotube forests," *Carbon*, vol. 196, pp. 391–400, 2022.

[44] J. Gallego, G. S. Gallego, C. Daza, R. Molina, J. B. C. Batiot-Dupeyat, and F. Mondragon, "Production of carbon nanotubes and hydrogen by catalytic ethanol decomposition," *Dyna*, vol. 80, pp. 78–85, 2013.

[45] I. Pelech, U. Narkiewicz, D. Moszyñski, and R. Pelech, "Simultaneous purification and functionalization of carbon

nanotubes using chlorination," *Journal of Materials Research*, vol. 27, no. 18, pp. 2368–2374, 2012.

[46] W. K. Maboya, N. J. Coville, and S. D. Mhlanga, "The synthesis of carbon nanomaterials using chlorinated hydrocarbons over a Fe-Co/$CaCO_3$ catalyst," *South African Journal of Chemistry*, vol. 69, pp. 15–26, 2016.

[47] W. K. Maboya, *Use of Chlorinated Carbon Materials to Make Nitrogen Doped and Un-doped Carbon Nanomaterials and Their Use in Water Treatment, Thesis and Dissertations*, University of the Witwatersrand, Johannesburg, South Africa, 2018.

[48] M. Arjmand and U. Sundararaj, "Electromagnetic interference shielding of nitrogen-doped and undoped carbon nanotube/polyvinylidene fluoride nanocomposites: a comparative study," *Composites Science and Technology*, vol. 118, pp. 257–263, 2015.

[49] D. Li, Y. Li, W. Song, and Y. Long, "Simultaneous determination of dihydroxybenzene isomers using disposable screen-printed electrode modified by multiwalled carbon nanotubes and gold nanoparticles," *Analytical Methods*, vol. 2, no. 7, pp. 837–843, 2010.

[50] R. Lv, Q. Li, A. R. Botello-Mendez et al., "Nitrogen-doped graphene: beyond single substitution and enhanced molecular sensing," *Scientific Reports*, vol. 2, no. 1, p. 586, 2012.

[51] H. R. Barzegar, E. Gracia-Espino, T. Sharifi, F. Nitze, and T. Wagberg, "Nitrogen doping mechanism in small diameter single-walled carbon nanotubes: impact on electronic properties and growth selectivity," *Journal of Physical Chemistry C*, vol. 117, no. 48, pp. 25805–25816, 2013.

[52] M. Arjmand and U. Sundararaj, "Effects of nitrogen doping on X-band dielectric properties of carbon nanotube/polymer nanocomposites," *ACS Applied Materials and Interfaces*, vol. 7, no. 32, pp. 17844–17850, 2015.

[53] M. Steinmetz, D. Lima, R. R. L. Machado et al., "Nitrogen-doped carbon nanotubes towards electrochemical sensing: effect of synthesis temperature," *Diamond and Related Materials*, vol. 110, Article ID 108093, 2020.

[54] R. R. L. Machado, T. A. Silva, T. M. C. dos Reis et al., "Electrochemical response of carbon paste electrodes modified with carbon nanotubes: effects of temperature of nitrogen doping and oxygen functionalization," *Diamond and Related Materials*, vol. 130, Article ID 109415, 2022.

[55] M.-Y. Yen, M.-C. Hsiao, S.-H. Liao et al., "Preparation of graphene/multiwalled carbon nanotube hybrid and its use as photoanodes of dye-sensitized solar cells," *ECS Meeting Abstracts*, vol. 49, no. 29, pp. 2005–3606, 2011.

[56] L. A. Goulart, R. Goncalves, A. A. Correa, E. C. Pereira, and L. H. Mascaro, "Synergic effect of silver nanoparticles and carbon nanotubes on the simultaneous voltammetric determination of hydroquinone, catechol, bisphenol A and phenol," *Microchimica Acta*, vol. 185, no. 1, p. 12, 2018.

[57] H.-L. Guo, S. Peng, J. Xu, Y. Zhao, and X. Kang, "Highly stable pyridinic nitrogen doped graphene modified electrode in simultaneous determination of hydroquinone and catechol," *Sensors and Actuators B: Chemical*, vol. 193, pp. 623–629, 2014.

[58] F. Wu, J. Zhao, D. Han, S. Zhao, R. Zhu, and G. Cui, "A three-electrode integrated electrochemical platform based on nanoporous gold for the simultaneous determination of hydroquinone and catechol with high selectivity," *Analyst*, vol. 146, no. 1, pp. 232–243, 2021.

[59] F. Haque, M. S. Rahman, E. Ahmed, P. K. Bakshi, and A. A. Shaikh, "A cyclic voltammetric study of the redox reaction of Cu(II) in presence of ascorbic acid in different pH media," *Dhaka University Journal of Science*, vol. 61, no. 2, pp. 161–166, 2013.

[60] Z. H. Sheng, X. Q. Zheng, J. Y. Xu, W. J. Bao, F. B. Wang, and X. H. Xia, "Electrochemical sensor based on nitrogen doped graphene: simultaneous determination of ascorbic acid, dopamine and uric acid," *Biosensors and Bioelectronics*, vol. 34, no. 1, pp. 125–131, 2012.

[61] A. Kabir, H. Yeasmin, M. A. Hasan et al., "Effect of pH on the Electrochemical Redox Behaviour of Co^{2+} in acetate buffer solution," *Dhaka University Journal of Science*, vol. 65, no. 2, pp. 107–112, 2017.

[62] A. K. Alkhawaldeh, "Platinum Nanoparticle electrode modified iodine using cyclic voltammetry and chronoamperometry for determination of ascorbic acid," *Analytical and Bioanalytical ElectroChemistry*, vol. 12, pp. 780–792, 2020.